Deuterium Toward WD 1634-573: Results from the Far Ultraviolet Spectroscopic Explorer (FUSE) Mission[1]

B. E. Wood,[2] J. L. Linsky,[2] G. Hébrard,[3] A. Vidal-Madjar,[3] M. Lemoine,[3] H. W. Moos,[4] K. R. Sembach,[4] and E. B. Jenkins[5]

ABSTRACT

We use *Far Ultraviolet Spectrocopic Explorer* (FUSE) observations to study interstellar absorption along the line of sight to the white dwarf WD 1634-573 ($d = 37.1 \pm 2.6$ pc). Combining our measurement of D I with a measurement of H I from *Extreme Ultraviolet Explorer* data, we find a D/H ratio toward WD 1634-573 of D/H = $(1.6 \pm 0.5) \times 10^{-5}$. In contrast, multiplying our measurements of D I/O I = 0.035 ± 0.006 and D I/N I = 0.27 ± 0.05 with published mean Galactic ISM gas phase O/H and N/H ratios yields $D/H_O = (1.2 \pm 0.2) \times 10^{-5}$ and $D/H_N = (2.0 \pm 0.4) \times 10^{-5}$, respectively. Note that all uncertainties quoted above are 2σ. The inconsistency between D/H_O and D/H_N suggests that either the O I/H I and/or the N I/H I ratio toward WD 1634-573 must be different from the previously measured average ISM O/H and N/H values. The computation of D/H_N from D I/N I is more suspect, since the relative N and H ionization states could conceivably vary within the LISM, while the O and H ionization states will be more tightly coupled by charge exchange.

Subject headings: white dwarfs — stars: individual (WD 1634-573) — ISM: abundances — ultraviolet: ISM

1. INTRODUCTION

The deuterium-to-hydrogen (D/H) ratio is of central importance to many areas of astrophysics. In the standard Big Bang cosmology, the primordial D/H value places strong constraints on the total baryon content in the universe. Since the deuterium abundance is believed to decrease with time due to the destruction of deuterium in stellar interiors, measurements of the local D/H value

[1]Based on observations made with the NASA-CNES-CSA Far Ultraviolet Spectroscopic Explorer. FUSE is operated for NASA by the Johns Hopkins University under NASA contract NAS5-32985.

[2]JILA, University of Colorado and NIST, Boulder, CO 80309-0440; woodb@casa.colorado.edu.

[3]Institut d'Astrophysique de Paris, CNRS, 98 bis Boulevard Arago, F-75014 Paris, France.

[4]Department of Physics and Astronomy, Johns Hopkins University, 3400 North Charles Street, Baltimore, MD 21218.

[5]Princeton University Observatory, Princeton, NJ 08544.

in our galaxy provide a lower limit for the primordial D/H value, while measurements of D/H in the Lyman-α forest provide an estimate that may be closer to the true primordial D/H ratio. Comparing the local and Lyman-α forest values provides a measure of how much stellar processing of material has occurred during the lifetime of the Milky Way Galaxy. Measurements of D/H in different locations in the Galaxy can provide critical tests of Galactic chemical evolution models.

The *Copernicus* satellite provided the first accurate D/H measurements within the Galactic ISM. Rogerson & York (1973) measured D/H = $(1.4 \pm 0.2) \times 10^{-5}$ toward β Cen, and York & Rogerson (1976) quoted an average value of D/H = $(1.8 \pm 0.4) \times 10^{-5}$ for several lines of sight observed by *Copernicus*. The Local Interstellar Cloud (LIC) within which the Sun resides appears to have D/H = $(1.5 \pm 0.1) \times 10^{-5}$ based on *Hubble Space Telescope* (HST) measurements along many lines of sight through the LIC (Linsky 1998), with no evidence for any significant variation within this small cloud (**?**, $\sim$ 7 pc across based on a compilation of LIC measurements;)]sr00. Estimating the primordial value from the Lyman-α forest has proved to be more difficult, although these measurements do suggest a higher D/H in the Lyman-α forest compared with the LIC, as one would expect (**?**, e.g.,)]jkw97,sb98,dt99,dk00. For a more thorough review of these intergalactic D/H measurements and how they relate to Galactic D/H, see Moos et al. (2001).

However, the LIC D/H value quoted above is also problematic, as it measures only very local interstellar gas. Values of D/H elsewhere in the Galaxy could in principle be much different, since material in different parts of the Galaxy has undergone varying amounts of stellar processing. Evidence for variations of D/H within the LISM have in fact been found for longer lines of sight sampling many clouds, based on data from HST and the IMAPS instrument (Vidal-Madjar et al. 1998; Jenkins et al. 1999; Sonneborn et al. 2000; Lemoine et al. 2001). Measuring the variation of D/H within the Galaxy is important both for determining the degree of mixing of ISM material within the Milky Way, and for determining a better estimate for the mean present day Galactic D/H value. Unfortunately, HST is not able to obtain measurements of D/H for long lines of sight through the Galaxy, because for column densities greater than 5×10^{18} cm^{-2} the H I Lyα absorption becomes so broad that it completely obscures the D I absorption.

Measuring deuterium at different locations throughout our Galaxy is one of the primary missions of the *Far Ultraviolet Spectroscopic Explorer* (FUSE). Unlike HST, FUSE can observe the higher lines of the H I Lyman series, which allows deuterium to be observed for higher ISM column densities. This paper is one of a series reporting the first deuterium measurements made with FUSE (Friedman et al. 2001; Hébrard et al. 2001; Kruk et al. 2001; Lehner et al. 2001; Lemoine et al. 2001; Sonneborn et al. 2001), including a summary paper of these initial results (Moos et al. 2001). The line of sight analyzed here is that toward the white dwarf WD 1634-573 (=HD 149499B). Table 1 lists properties of our target star, which is a very metal poor DO white dwarf unlikely to have photospheric metal lines contaminating the ISM absorption lines in which we are interested (Dreizler 1999). There is a K0 V companion star (HD 149499A) that will be in the FUSE aperture for our observations. However, even though this star is believed to be quite active (Jordan et al. 1997), emission from this star will not be detectable against the very bright continuum of the hot

white dwarf, based on extrapolations of H I Lyman line fluxes observed for other active single K dwarfs.

With a path length of only 37.1 ± 2.6 pc (Perryman et al. 1997), the WD 1634-573 line of sight does not exceed the distance scale of deuterium measurements accessible to HST. However, the H I column density estimated from *Extreme Ultraviolet Explorer* (EUVE) data is $N_{\rm H} = (7 \pm 2) \times 10^{18}$ cm^{-2} (Napiwotzki et al. 1996), too high for deuterium to be detectable in Lyα, so this line of sight *does* extend deuterium measurements to higher columns than are measurable with HST.

2. FUSE OBSERVATIONS

The DO white dwarf WD 1634-573 has been observed by FUSE three times through the low resolution (LWRS) aperture and twice through the medium resolution (MDRS) aperture. These observations are listed in Table 2. Collectively, the LWRS data set consists of 28 separate exposures with a total exposure time of 19,406 s, while the MDRS data set consists of 37 separate exposures totaling 18,225 s.

In order to fully cover its 905–1187 Å spectral range, FUSE has a multi-channel design — two channels (LiF1 and LiF2) use Al+LiF coatings, two channels (SiC1 and SiC2) use SiC coatings, and there are two different detectors (A and B). For a full description of the instrument, see Moos et al. (2000). With this design FUSE acquires spectra in eight segments covering different, overlapping wavelength ranges. For both of the LWRS and MDRS data sets, the individual exposures processed in the standard FUSE pipeline (version 1.6.9) are cross-correlated and coadded to create a single spectrum for each segment. We decided not to coadd the individual segments to ensure that such an operation would not degrade the spectral resolution. Instead, a spectrum covering the full FUSE spectral range is spliced together from several different segments. To be more precise, the spectrum combines the following segments: SiC1B (910–925 Å), SiC2A (925–995 Å), LiF1A (995–1075 Å), SiC2B (1075–1095 Å), and LiF2A (1095–1180 Å).

We keep the LWRS and MDRS spectra separate, since the spectral resolution of the two may be slightly different. This also gives us two separate spectra that we can analyze independently to see if we obtain the same answer from both data sets (see below). One exception is the H I Lyβ line at 1025 Å. For the LWRS spectrum, there is substantial contamination from airglow emission in this line, which is not the case in the MDRS data thanks to the narrower aperture. Thus, we import the MDRS Lyβ line into the LWRS spectrum to allow the analysis of the LWRS data to also consider this important line. Airglow is also a potential contaminant for many of the O I and N I lines (Feldman et al. 2001), but the continuum fluxes of WD 1634-573 are high enough to overwhelm the airglow and we see no difference in the LWRS and MDRS spectra that would suggest a problem.

Since there is no wavelength calibration lamp onboard FUSE, the wavelength scale produced by the FUSE data reduction pipeline is very uncertain. Thus, we identify many ISM absorption

lines throughout the LWRS and MDRS spectra and measure their centroids. For each segment, the average shift between the centroids and rest wavelengths of lines within that segment is used to correct the wavelength scale and place it in the rest frame of the interstellar absorption.

Figure 1 shows the resulting reduced spectrum for the LWRS data. Coadding the separate exposures of these segments helps to suppress fixed pattern noise somewhat. However, the spectrum in Figure 1 shows that significant periodic fixed pattern noise remains in many locations, in particular the moiré pattern mentioned by Sahnow et al. (2000) that produces noise with a period of about nine pixels. The effective signal-to-noise of our spectrum is in many locations limited by the moiré ripples rather than actual photon noise.

3. ANALYSIS

3.1. GHRS Data

Obtaining the most accurate measurements for column densities requires that the number of ISM absorption components along the line of sight be known with some precision. Unfortunately, FUSE does not have sufficient spectral resolution to resolve the ISM velocity structure unless the components are very widely separated, and there are also no high resolution HST or ground based data to provide this information. There are, however, a few moderate resolution HST spectra of WD 1634-573 taken on 1996 September 3 with the G160M grating of the Goddard High Resolution Spectrograph (GHRS) instrument formerly on board HST, and these spectra contain a few ISM lines (Dreizler 1999). In Figure 2, we plot the ISM absorption lines of S II λ1259.519 and Si II λ1260.422 on a heliocentric velocity scale. We have fitted the S II line with a single absorption component, with a correction for instrumental broadening assuming a Gaussian instrumental profile with a width of 4.4 pixels (Gilliland 1994).

The S II line is centered at -19.6 km s^{-1}, which is very close to the velocity predicted by the LIC vector (Lallement et al. 1995), -18.9 km s^{-1}. Actually, with Galactic coordinates of $l = 329.9°$ and $b = -7.0°$, the WD 1634-573 line of sight is more likely to sample the so-called "G cloud," a proposed very nearby cloud in the Galactic Center direction very similar to the LIC in most respects, but which has a slightly different flow vector (Lallement & Bertin 1992; Wood, Linsky, & Zank 2000). The G cloud vector predicts a velocity of -21.2 km s^{-1}, a bit farther from the measured value of -19.6 km s^{-1} than the LIC value, but still close enough to be consistent considering this is moderate rather than high resolution data.

However, when the stronger, opaque Si II λ1259.519 line is fitted with a single absorption component, the measured absorption centroid is -15.2 km s^{-1}, a 4.4 km s^{-1} discrepancy with S II. An analogous effect is detectable in the FUSE data, where optically thick lines also appear to be redshifted relative to optically thin lines nearby in the spectrum. This fact strongly suggests the presence of at least one extra velocity component along the line of sight, which is redshifted

relative to the primary absorption component. Thus, in Figure 2 the Si II line is fitted with two components, one with a velocity fixed at the velocity suggested by the S II line, and the other located redward of the main component by 17 km s^{-1} to account for the extra absorption on that side of the line. The Doppler broadening parameters are forced to be the same for both components to reduce the number of free parameters.

Unfortunately, at the resolution of the GHRS G160M grating ($R \approx 20,000$) the ISM lines are not resolved any more than they are for FUSE, so the true velocity structure of the WD 1634-573 line of sight is still unknown. The fit to the Si II line in Figure 2 suggests at least one additional component redward of the primary component, but the fit is not quantitatively useful for accurately estimating component velocity separations or column density ratios.

3.2. Fitting the FUSE Data

Figure 1 provides a broad overview of the WD 1634-573 spectrum using the LWRS data. Figure 3 shows closeups of many of the ISM absorption lines using MDRS data. The WD 1634-573 spectral regions shown in Figure 1 contain all of the absorption lines that we use to derive interstellar column densities for this line of sight for various elements. At least 21 H I Lyman lines are observable, from Lyβ at 1025 Å down to the numerous H I lines clustered near the Lyman limit at 912 Å. The six strongest Lyman lines are plotted in Figure 4 on a velocity scale centered on the H I absorption, showing that deuterium (D I) absorption is detectable at about -82 km s^{-1} in at least the strongest four lines (Lyβ through Lyϵ).

Many O I and N I lines of varying strengths are also apparent in the FUSE spectrum (see Fig. 1), meaning FUSE data should provide accurate measurements of O I and N I column densities. Other atomic species with at least one detectable ISM line are N II, P II, C II, C III, Ar I, Fe II, and perhaps Si II. The Si II λ989 line may be blended with a N III line at that location (Jenkins et al. 2000) and its strength seems to be inconsistent with the nondetection of Si II λ1020, so that identification is listed with a question mark in Figure 1.

As described by Moos et al. (2001), the first FUSE D/H analyses published in this series of articles are all the result of at least two independent analyses, and the study of WD 1634-573 presented here is no exception. This approach of using independent analyses with significantly different methods is the best way to estimate the magnitude of systematic errors, which are very difficult to quantify otherwise. The final column densities that we derive are compromise values consistent with the results of both of these independent analyses. Several of us (G. H., M. L., and A. V.-M.) analyzed the WD 1634-573 data in a manner very similar to the analysis of the WD 2211-495 line of sight described by Hébrard et al. (2001), and we refer the reader to that paper for a thorough description. We now describe the other independent analysis in far more detail.

In order to analyze the absorption lines, we first estimate the stellar continuum overlying the absorption. This is done with a series of polynomial fits covering the entire FUSE spectrum.

The result is shown in Figure 1. Estimating the continuum above the Lyβ λ1025 absorption requires a little more work because of the significant amount of absorption in the line wings. This wing absorption indicates that the Lorentzian wings of the opacity profile are starting to become important, which in turn signifies that the line is no longer completely in the flat part of the curve of growth. Our initial guess for the background continuum assumed no wing absorption. After the initial fit was performed (as described below), the fit to the Lyβ spectral region was poor because of the presence of wing absorption, so the residuals of that fit were used to derive a higher continuum that would improve the quality of the fit. Another iteration leads to the Lyβ continuum shown in Figures 1 and 4.

Our fits to the absorption lines are global fits, where all the lines are fitted simultaneously. We use Morton (1991) as our primary source for the necessary atomic data and Verner, Barthel, & Tytler (1994) for some of the higher H I Lyman lines. Note that we use the Morton (1991) line list available on the WWW (`http://www.hia.nrc.ca/staff/dcm/atomic_data.html`), for which many of the N I oscillator strengths have been updated from their original published values. All clearly detected lines are identified in Figure 1 and also listed in Table 3 along with rest wavelengths and oscillator strengths. Table 3 lists equivalent widths for the lines, except for cases where blending is too severe for an accurate measurement. The equivalent widths and quoted 2σ uncertainties are based on measurements of both the LWRS and MDRS spectra, assuming several different background continua estimations.

However, in our fits not only are the detected lines included, but we also consider many undetected lines of atomic species with at least one detected line. These nondetections can provide useful upper limit constraints for our fitting routine. There are two O I lines listed by Morton (1991) that we do *not* include in our fits because their listed f values suggest line strengths that are clearly inconsistent with the observations, based on comparison with the other O I lines seen in the spectrum. These are the O I λ972.1 and λ1026.5 lines. The oscillator strengths listed for these two lines must be incorrect.

The primary free parameters of the global fit are the column densities of the various atomic species (H I, D I, O I, N I, etc.). For all detected and unblended lines, we allow the centroid of the line to vary as a free parameter of the fit to account for inaccuracies in the wavelength calibration. The temperature (T) and nonthermal velocity (ξ) of the interstellar gas are also free parameters. The Doppler broadening parameters (b) of the various ISM lines are computed from T and ξ using the equation $b^2 = 0.0165T/A + \xi^2$, where A is the atomic weight of the atomic species associated with each line. Note, however, that because the lines are not resolved and because we cannot accurately account for the multiple velocity components present in the lines (see §3a), the validity of the T and ξ values derived in our fits is questionable.

In Figures 1 and 3, a single-component global fit to the absorption lines is shown both before (dotted line) and after (thick solid line) convolution with the instrumental profile. Figure 1 shows a fit to the LWRS data and Figure 3 shows a fit to the MDRS data. Unfortunately, the instrumental

profile, or line spread function (LSF), is not currently well known for FUSE, and may in any case conceivably vary from one observation to the next depending on the accuracy of the pointing for that particular observation and on how accurately the individual exposures are cross-correlated and coadded (Kruk et al. 2001). Thus, the LSF is a free parameter of our fit. We assume a two-Gaussian representation for the LSF, which we assume to be applicable over the entire FUSE spectral region. This is just an approximation, however, as the LSF undoubtedly varies with wavelength.

The fits in Figures 1 and 3 are single-component fits performed as described above. In order to decide on the final column density values and their uncertainties, however, we experiment with many other fits. Analyzing the LWRS and MDRS spectra independently provides some sense of the systematic uncertainties involved in the fitting process. We also experiment with different estimates for the continuum placement. Particularly for the D I lines, we also try fits without considering the H I lines at all. This allows us to more simply extrapolate a continuum just over the D I lines themselves rather than making the more uncertain extrapolation over both the D I and H I lines, which are partially blended for Lyβ and Lyγ (see Fig. 4). There is significant potential for systematic error with regards to D I since all the D I lines are just blueward of H I lines, which makes continuum placement tricky. The fact that photospheric He II and H I absorption are centered at these locations also complicates matters (Napiwotzki et al. 1995).

Finally, we also experiment with various two-component fits. These fits all assume a weaker second component redward of the primary component, as suggested by the Si II fit in Figure 2, but we experiment with different velocity separations and column density ratios for the two components. The column density ratio is typically assumed to be the same for all lines of all atomic species in order to limit the number of free parameters. We also typically assume that the T and ξ values are identical for both components. We do not think that the FUSE or GHRS data have sufficient resolution to accurately derive T and ξ at all, let alone for both components separately. Nevertheless, we experimented with fits allowing T and ξ to be different for the two components and our total column density measurements do not change significantly. The fit to the data shown in Figure 4 is an example of one of the global two-component fits, although only the six strongest Lyman lines are shown in the figure. This particular fit assumes a velocity separation of 17 km s^{-1} and a very large column density ratio of 250:1 for the two components, explaining why the second component (dashed lines) is only seen for the H I lines and not the optically thin D I lines.

As described above, a two-Gaussian LSF is a free parameter of our fits. In Figure 5, we show examples of LSFs that were derived for various fits, not only to the WD 1634-573 data but also to FUSE observations of another white dwarf, WD 2211-495, which are analyzed in detail by Hébrard et al. (2001). The solid lines are LSFs derived from fits to the LWRS data, and the dotted lines are LSFs from the MDRS data. There is significant scatter in the estimated LSF shape, which indicates the level of uncertainty in this average FUSE LSF, and it should also be pointed out once again that the real FUSE LSF will be wavelength dependent. There is no obvious systematic difference between the LWRS and MDRS profiles, and there are not any obvious systematic differences between the LSFs derived from the WD 1634-573 and WD 2211-495 data sets. The dashed line in Figure 5 is

the average of all these LSFs, which can be approximated by the sum of two Gaussians with the following parameters: $\lambda_1 = 0.01$ pix, $FWHM_1 = 10.40$ pix, and $A_1 = 0.879$ for the first Gaussian, and $\lambda_2 = 0.82$ pix, $FWHM_2 = 25.26$ pix, and $A_2 = 0.117$ for the second (λ=centroid position, $FWHM$=full width at half-maximum, and A=amplitude). The width of this average LSF suggests a spectral resolution of $R \equiv \lambda/\Delta\lambda \approx 15,000$.

The FUSE LSF has broad wings, which is the reason the flux in the saturated core of the broad H I Lyman absorption lines does not fall to zero (see Figs. 1, 3, and 4). The prominence of the line wings of our derived LSFs is determined almost entirely from the Lyman lines. When we fit the data without the H I lines (see above), the broad wings disappear since the remaining lower opacity line profiles are not nearly as sensitive to the far wings of the LSF.

In reality, the FUSE LSF will vary with wavelength, so we tried fits with the LSF allowed to vary within the spectrum. These trials did not yield fit parameters statistically different from those obtained assuming an invariable LSF. However, it should be pointed out that there is not enough information within the data to accurately determine a wavelength dependent LSF, so our attempt to do so may not have fully accounted for systematic errors associated with the wavelength dependence of the true LSF. Variability in the LSF could be at least partially responsible for the discrepancies in the fits to the H I lines in Figure 4. Kruk et al. (2001) present further, detailed discussion about the difficulties in estimating the LSF for FUSE data.

All of the various fits that we try using different continua, different data sets (i.e., LWRS or MDRS), and different types of multi-component fits are visually inspected to make sure the spectra are fitted reasonably well. After visibly poor quality fits are thrown out, we are left with a collection of fits that we can use to determine the column densities and their uncertainties. For each column density, we have from these fits a set of measured columns that lead to acceptable fits to the data. This set defines a range of acceptable values for that column density. We choose the center of that range as our best estimate for the column density and the half-width of the range as the estimated uncertainty.

For example, our set of $\log$ N(N I) values from various acceptable fits is [14.51, 14.52, 14.59, 14.60, 14.61, 14.64, 14.66, 14.67, 14.71], where for the sake of brevity we have omitted repetition of identical $\log$ N(N I) measurements. From this set of numbers, we estimate $\log$ N(N I) $= 14.61 \pm 0.10$ since 14.61 is at the center of the range of values and 0.10 is the half-width of the range. Uncertainties estimated in this manner are not statistical errors, but we consider them to be something like 2σ uncertainties in the sense of being roughly 95% confidence intervals. They certainly are more conservative than "1σ uncertainties" since we do not throw out 32% of our acceptable fits before estimating the errors. The temperatures we find with our fits are in the $T = 4800 - 7500$ K range and the nonthermal velocities are in the range $\xi = 0 - 5$ km s^{-1}. However, as noted above the presence of multiple components complicates the interpretation of these quantities.

As mentioned near the beginning of this section, we performed a second independent analysis

of the data using a different technique. This technique uses a spectral fitting code called Owens.f, developed by one of us (M. L.) and the FUSE French team. A thorough description of the use of this code can be found in Hébrard et al. (2001), another of this series of papers on the first deuterium measurements with FUSE, which describes the measurement of deuterium toward WD 2211-495. The Owens code performs global fits to many absorption lines simultaneously by χ^2 minimization. All the data from different FUSE channels and different observations are fitted simultaneously, allowing for redundant coverage of a given spectral line. The background continuum for each line, represented as a polynomial, is left as a free parameter of the fit. The width of the LSF is allowed to vary independently for each line to try to account for expected LSF variations with wavelength in the FUSE spectra. Only the optically thin lines are included in the fit in order to avoid systematic errors associated with the structure of the line of sight and incorrect knowledge of the LSF. Uncertainties (2σ) are estimated from an analysis of $\Delta\chi^2$ contours (**?**, see)]gh01. The best fit yielded a $\chi^2 = 3629.1$ with 3076 degrees of freedom.

Despite the differences between the two fitting procedures, the results are consistent, with overlapping error bars. The final column density measurements and 2σ uncertainties listed in Table 4 represent a synthesis of these two independent analyses, and are consistent with the results of both. We do not list a Si II column density because of the possible blend with N III (see above). The Si II λ1260 line observed by HST/GHRS (see Fig. 2) is saturated and therefore does not provide a precise column density, but the S II λ1259 line (see Fig. 2) and a weaker S II λ1253 line do provide a useful S II column density that we list in Table 4 for completeness.

4. DISCUSSION

Because there are many D I, N I, and O I lines of varying strengths, we believe our column density measurements for these species are quite accurate, with 2σ uncertainties of only 0.05–0.07 dex (see Table 4). The uncertainty roughly doubles when we have only one or two unsaturated lines to work with, as is the case for P II, S II, Ar I, and Fe II. When we have only saturated lines to work with, the uncertainties are much higher. Thus, the H I, C II, C III, and N II column densities have uncertainties in the 0.3–0.7 dex range.

This problem with saturated lines exists for H I despite there being many lines to work with, at least one of which (H I Lyβ) is at least partly out of the flat part of the curve of growth (see above). Nevertheless, our analysis suggests that FUSE data cannot be used to derive a precise H I column density toward WD 1634-573. The situation will likely be better for higher column density lines of sight with at least Lyβ and Lyγ completely out of the flat part of the curve of growth. However, Lemoine et al. (2001) express concern that undetected hot H I components, such as the heliospheric and astrospheric absorption previously observed toward nearby cool stars (Wood et al. 2000), could potentially affect any measurement of H I column densities from the Lyman absorption lines, making it even harder to assess systematic errors for these analyses.

Because our H I measurement ($\log \mathrm{N(H\ I)} = 18.6 \pm 0.4$) is not very precise, we must look elsewhere for an H I measurement that we can use to compute an accurate D/H value for this line of sight. Holberg, Barstow, & Sion (1998) estimated $\log \mathrm{N(H\ I)} \approx 18.8$ from their analysis of IUE observations of the Lyα line. Napiwotzki et al. (1995) found $\log \mathrm{N(H\ I)} = 19.0 \pm 0.4$ from ORFEUS observations of the same H I Lyman lines that we have analyzed using FUSE. Our results are consistent with ORFEUS, but the error bars are large for both measurements. The most accurate measurement appears to be from EUVE observations of H I Lyman continuum absorption shortward of 912 Å. In a simultaneous analysis of both ORFEUS and EUVE data, which allowed both photospheric parameters (e.g., T_{eff} and $\log g$) and the interstellar H I column density to vary, Napiwotzki et al. (1996) finds $\mathrm{N(H\ I)} = (7 \pm 2) \times 10^{18}$ cm^{-2} (i.e., $\log \mathrm{N(H\ I)} = 18.85 \pm 0.12$). See also Jordan et al. (1997) for more details on the photospheric analysis. Based on this H I value and our D I measurement ($\log \mathrm{N(D\ I)} = 14.05 \pm 0.05$), which are both quoted with 2σ uncertainties, we find that $\mathrm{D/H} = (1.6 \pm 0.5) \times 10^{-5}$ toward WD 1634-573. This value is consistent with the LIC value of $\mathrm{D/H} = (1.5 \pm 0.1) \times 10^{-5}$ (Linsky 1998).

The Ar I/H I abundance ratio, $\log \mathrm{Ar\ I/H\ I} = -5.59 \pm 0.17$, is close to the B star Ar abundance of $\log \mathrm{Ar/H} = -5.50$ (Holmgren et al. 1990). This is in contrast to the results of Jenkins et al. (2000), who found significantly lower Ar I/H I ratios toward 3 stars ($\log \mathrm{Ar\ I/H\ I} \approx -5.9$), which they attributed to a higher ionization state of Ar compared with H due to the high photoionization cross section of Ar. This provides important evidence that the LISM is in fact in photoionization equilibrium. Perhaps the WD 1634-573 line of sight is more shielded from photoionization, allowing the ionization state of Ar to be closer to that of H. The apparently high N II/N I ratio (see Table 4) might suggest otherwise, although uncertainty in the N II column is large.

Due to charge exchange interactions, the ionization states of D, H, and O are closely coupled. This means that the total D/O gas phase abundance ratio is well approximated by the D I/O I ratio. Charge exchange is also important between D, H, and N, although to a lesser extent, so $\mathrm{D/N} \approx \mathrm{D\ I/N\ I}$. Our measurements of D I, O I, and N I in Table 4 yield $\mathrm{D\ I/O\ I} = 0.035 \pm 0.006$ and $\mathrm{D\ I/N\ I} = 0.27 \pm 0.05$ (2σ errors).

These ratios can be used to estimate D/H when we multiply them by previously measured values for the gas phase O/H and N/H ratios in the ISM. Meyer, Jura, & Cardelli (1998) used GHRS observations of the O I λ1356 lines of 13 OB stars that are more distant ($d = 100 - 1000$ pc) than WD 1634-573 to estimate $\mathrm{O/H} = (3.43 \pm 0.15) \times 10^{-4}$, with no evidence for variation within the ISM. Note that we have increased the published O/H value by 7.5% to account for a revised f value for O I λ1356 suggested by Welty et al. (1999). Likewise, Meyer, Cardelli, & Sofia (1997) find $\mathrm{N/H} = (7.5 \pm 0.4) \times 10^{-5}$ toward a similar sample of 7 OB stars, also with no evidence of variation. Note that these measurements of O/H and N/H only consider the column densities of O I, N I, H I, and H_2, and do not take into account the column densities of the ionized species O II, N II, or H II. Since $\mathrm{O\ I/O\ II} = \mathrm{H\ I/H\ II}$ is a good approximation, the O/H value should be relatively free from inaccuracies induced by ionization state issues, but the N/H value is potentially susceptible to differences and variations in the relative ionization states of N and H (see above). Note also that

the cited uncertainties in O/H and N/H are 1σ standard deviations of the mean rather than simple standard deviations about the mean, meaning that the scatter of the individual O/H and N/H measurements is actually larger than suggested by the quoted uncertainties, potentially allowing for a larger variation of O/H and N/H within the ISM than is suggested by those uncertainties.

In any case, multiplying our D I/O I measurement with the Meyer et al. (1998) mean O/H value results in $D/H_O = (1.2 \pm 0.2) \times 10^{-5}$, while multiplying our D I/N I measurement with the Meyer et al. (1997) mean N/H value results in $D/H_N = (2.0 \pm 0.4) \times 10^{-5}$ (2σ errors). These two D/H values do not overlap, suggesting that the either the O I/H I and/or N I/H I ratio toward WD 1634-573 is not consistent with the Meyer et al. (1997, 1998) mean O/H and N/H values. As suggested above, the N I/H I ratio is more suspect due to the possibility of variations in the relative ionization states of N and H within the LISM. Furthermore, the N I/H I value measured toward G191-B2B is clearly lower than the Meyer et al. (1997) N/H value (Vidal-Madjar et al. 1998; Lemoine et al. 2001). A more extensive discussion of these issues is provided by Moos et al. (2001). Note that the D/H_O measurement is a bit lower than the accepted LIC value of $D/H = (1.5 \pm 0.1) \times 10^{-5}$.

5. SUMMARY

We have used FUSE observations to measure column densities for many atomic species toward the white dwarf WD 1634-573, which are listed in Table 4. These measurements and uncertainties represent a synthesis between the results of two separate, independent analyses. We feel the use of independent analyses is the best possible method for assessing the magnitude of systematic errors in this type of study. Of particular significance is the measurement of D I, because of the importance of the deuterium-to-hydrogen (D/H) ratio for cosmology and studies of Galactic chemical evolution. We find that a previously published value for the H I column density from EUVE is more precise than what we can measure from FUSE, although our FUSE measurement is consistent with the EUVE result. Combining the FUSE D I column density with the EUVE H I column density yields $D/H = (1.6 \pm 0.5) \times 10^{-5}$ (2σ uncertainty), consistent with the LIC value of $D/H = (1.5 \pm 0.1) \times 10^{-5}$ (Linsky 1998). Combining our WD1634-573 measurement with others in this first series of FUSE D/H measurements in the LISM, Moos et al. (2001) find that $D/H = (1.51 \pm 0.07) \times 10^{-5}$ within the Local Bubble, which extends ~ 100 pc from the Sun in most directions. There is no evidence for variation within the Local Bubble, but the dispersion of Galactic D/H measurements increases significantly if IMAPS and *Copernicus* measurements of longer lines of sight are considered.

We can also estimate D/H for WD1634-573 by computing D I/O I and D I/N I ratios from our FUSE measurements, and multiplying them by mean gas phase O/H and N/H ratios derived for the ISM by Meyer et al. (1997, 1998). However, these yield inconsistent D/H values, suggesting that either O I/H I and/or N I/H I toward WD 1634-573 is not consistent with the O/H and N/H ratios from Meyer et al. (1997, 1998). The N I/H I value is the more likely culprit since the ionization state of N is more likely to vary relative to H than is the case for O, and the work of Vidal-Madjar et al. (1998) and Lemoine et al. (2001) shows that N I/H I toward G191-

B2B is significantly lower than the Meyer et al. (1997) N/H value. The D/H value computed from D I/O I and O/H, $D/H_O = (1.2 \pm 0.2) \times 10^{-5}$, is slightly lower than the LIC value quoted above. We note that the published O/H and N/H values for the ISM are mean values derived from observations of stars located much farther away than WD 1634-573 ($d = 37.1 \pm 2.6$ pc) and thus may not be representative of gas in the nearby ISM. The importance of FUSE D I/O I and D I/N I measurements is discussed further by Moos et al. (2001).

We would like to thank R. Napiwotzki for information about his EUVE and ORFEUS studies of WD 1634-573, and we would like to thank J. C. Howk and D. York for useful comments on the manuscript. This work is based on data obtained for the Guaranteed Time Team by the NASA-CNES-CSA FUSE mission operated by the Johns Hopkins University. Financial support to U. S. participants has been provided by NASA contract NAS5-32985. French participants are supported by CNES. The first author is supported in part by NASA grant NAG5-9041 to the University of Colorado.

REFERENCES

Burles, S., & Tytler, D. 1998, ApJ, 499, 699

Dreizler, S. 1999, A&A, 352, 632

Feldman, P. D., Sahnow, D. J., Kruk, J. W., Murphy, E. M., & Moos, H. W. 2001, J. Geophys. Res., in press

Friedman, S. D., et al. 2001, ApJS, submitted

Gilliland, R. L. 1994, GHRS Instrument Science Report 063 (Baltimore: STScI)

Hébrard, G., et al. 2001, ApJS, submitted

Holberg, J. B., Barstow, M. A., & Sion, E. M. 1998, ApJS, 119, 207

Holmgren, D. E., Brown, P. J. F., Dufton, P. L., & Keenan, F. P. 1990, ApJ, 364, 657

Jenkins, E. B., et al. 2000, ApJ, 538, L81

Jenkins, E. B., Tripp, T. M., Wozniak, P. R., Sofia, U. J., & Sonneborn, G. 1999, ApJ, 520, 182

Jordan, S., Napiwotzki, R., Koester, D., & Rauch, T. 1997, A&A, 318, 461

Kirkman, D., Tytler, D., Burles, S., Lubin, D., & O'Meara, J. M. 2000, ApJ, 529, 655

Kruk, J. W., et al. 2001, ApJS, submitted

Lallement, R., & Bertin, P. 1992, A&A, 266, 479

Lallement, R., Ferlet, R., Lagrange, A. M., Lemoine, M., & Vidal-Madjar, A. 1995, A&A, 304, 461

Lehner, N., et al. 2001, ApJS, submitted

Lemoine, M., et al. 2001, ApJS, submitted

Linsky, J. L. 1998, Space Sci. Rev., 84, 285

Meyer, D. M., Cardelli, J. A., & Sofia, U. J. 1997, ApJ, 490, L103

Meyer, D. M., Jura, M., & Cardelli, J. A. 1998, ApJ, 493, 222

Moos, H. W., et al. 2000, ApJ, 538, L1

Moos, H. W., et al. 2001, ApJS, submitted

Morton, D. C. 1991, ApJS, 77, 119

Napiwotzki, R., Hurwitz, M., Jordan, S., Bowyer, S., Koester, D., Weidemann, V., Lampton, M., & Edelstein, J. 1995, A&A, 300, L5

Napiwotzki, R., Jordan, S., Bowyer, S., Hurwitz, M., Koester, D., Rauch, T., & Weidemann, V. 1996, in Astrophysics in the Extreme Ultraviolet, ed. S. Bowyer & R. F. Malina (Dordrecht: Kluwer), 241

Perryman, M. A. C., et al. 1997, A&A, 323, L49

Redfield, S., & Linsky, J. L. 2000, ApJ, 534, 825

Rogerson, J. B., & York, D. G. 1973, ApJ, 186, L95

Sahnow, D. J., et al. 2000, ApJ, 538, L7

Sonneborn, G., et al. 2001, ApJS, submitted

Sonneborn, G., Tripp, T. M., Ferlet, R., Jenkins, E. B., Sofia, U. J., Vidal-Madjar, A., & Wozniak, P. R. 2000, ApJ, 545, 277

Tytler, D., Burles, S., Lu, L., Fan, X. M., Wolfe, A., & Savage, B. D. 1999, AJ, 117, 63

Verner, D. A., Barthel, P. D., & Tytler, D. 1994, A&AS, 108, 287

Vidal-Madjar, A., et al. 1998, A&A, 338, 694

Webb, J. K., Carswell, R. F., Lanzetta, K. M., Ferlet, R., Lemoine, M., Vidal-Madjar, A., & Bowen, D. V. 1997, Nature, 388, 250

Welty, D. E., Hobbs, L. M., Lauroesch, J. T., Morton, D. C., Spitzer, L., & York, D. G. 1999, ApJS, 124, 465

Wood, B. E., Linsky, J. L., & Zank, G. P. 2000, ApJ, 537, 304

York, D. G., & Rogerson, J. B. 1976, ApJ, 203, 378

AAS LaTeX macros v5.0.

Table 1. WD 1634-573 Properties

Property	Value
Other Name	HD 149499B
Spectral Type	DO
RA (2000)	16:38:30
DEC (2000)	$-57°28.2'$
Gal. long. (deg)	329.9
Gal. lat. (deg)	-7.0
V	11.7
B–V	-0.39
Distance (pc)	37.1 ± 2.6[a]
T_{eff} (K)	$49,500 \pm 500$[b]
$\log g$	7.97 ± 0.08[b]

[a]Perryman et al. (1997).

[b]Napiwotzki et al. (1995).

Table 2. FUSE Observations

Observation ID	Date	Aperture	# of Exposures	Exp. Time (s)
M1031101	2000 March 30	LWRS	8	5396
M1031102	2000 April 12	LWRS	8	5448
M1031103	2000 May 16	LWRS	12	8562
S5140201	2000 April 13	MDRS	23	11,464
M1031104	2000 May 17	MDRS	14	6761

Table 3. Detected ISM Lines

Ion	λ_{rest}	f	W_λ (mÅ)[a]	Ion	λ_{rest}	f	W_λ (mÅ)[a]
H I	913.480	1.29×10^{-4}	···	N I	953.970	3.36×10^{-2}	31.6 ± 4.6
H I	913.641	1.49×10^{-4}	···	N I	954.104	4.43×10^{-3}	13.9 ± 5.0
H I	913.826	1.70×10^{-4}	···	N I	963.990	1.61×10^{-2}	25.5 ± 3.5
H I	914.039	1.97×10^{-4}	···	N I	964.626	1.04×10^{-2}	14.9 ± 8.5
H I	914.286	2.30×10^{-4}	149.3 ± 12.4	N I	965.041	5.13×10^{-3}	14.2 ± 2.1
H I	914.576	2.71×10^{-4}	154.7 ± 2.7	N I	1134.165	1.34×10^{-2}	32.0 ± 6.6
H I	914.919	3.21×10^{-4}	158.3 ± 5.1	N I	1134.415	2.68×10^{-2}	38.1 ± 6.7
H I	915.329	3.87×10^{-4}	157.7 ± 2.8	N I	1134.980	4.02×10^{-2}	43.1 ± 8.3
H I	915.824	4.69×10^{-4}	156.1 ± 22.8	N II	915.613	1.45×10^{-1}	50.6 ± 14.7
H I	916.429	5.78×10^{-4}	171.7 ± 6.5	N II	1083.991	1.03×10^{-1}	63.3 ± 5.0
H I	917.181	7.23×10^{-4}	171.0 ± 9.1	O I	916.815	4.05×10^{-4}	6.6 ± 1.8
H I	918.129	9.21×10^{-4}	184.7 ± 10.2	O I	919.658	8.13×10^{-4}	14.0 ± 5.2
H I	919.351	1.21×10^{-3}	182.1 ± 6.2	O I	921.860	1.12×10^{-3}	14.3 ± 3.5
H I	920.963	1.60×10^{-3}	200.1 ± 2.6	O I	924.952	1.59×10^{-3}	22.8 ± 1.7
H I	923.150	2.22×10^{-3}	189.7 ± 17.8	O I	925.442	3.54×10^{-4}	5.0 ± 3.0
H I	926.226	3.18×10^{-3}	204.9 ± 6.5	O I	929.517	2.36×10^{-3}	27.2 ± 5.3
H I	930.748	4.82×10^{-3}	217.5 ± 4.5	O I	930.257	5.37×10^{-4}	8.2 ± 3.0
H I	937.804	7.80×10^{-3}	224.6 ± 6.1	O I	936.630	3.73×10^{-3}	36.2 ± 3.0
H I	949.743	1.39×10^{-2}	236.6 ± 7.8	O I	948.685	6.45×10^{-3}	39.7 ± 4.8
H I	972.537	2.90×10^{-2}	257.5 ± 13.7	O I	950.885	1.57×10^{-3}	19.2 ± 5.4
H I	1025.722	7.91×10^{-2}	378.6 ± 21.2	O I	971.738	1.48×10^{-2}	50.9 ± 3.7
D I	937.548	7.81×10^{-3}	2.5 ± 2.0	O I	976.448	3.30×10^{-3}	34.1 ± 4.0
D I	949.485	1.40×10^{-2}	7.2 ± 3.2	O I	988.578	5.42×10^{-4}	···
D I	972.272	2.90×10^{-2}	18.1 ± 4.8	O I	988.655	7.71×10^{-3}	···
D I	1025.443	7.91×10^{-2}	33.9 ± 4.2	O I	988.773	4.32×10^{-2}	···
C II	1036.337	1.23×10^{-1}	83.5 ± 15.7	O I	1039.230	9.20×10^{-3}	46.3 ± 8.3
C III	977.020	7.62×10^{-1}	103.7 ± 9.6	Si II?	989.873	1.33×10^{-1}	36.5 ± 7.9
N I	952.303	1.76×10^{-3}	3.0 ± 2.0	P II	963.801	1.46×10^{0}	10.0 ± 3.0
N I	952.415	1.56×10^{-3}	2.0 ± 1.5	Ar I	1048.220	2.44×10^{-1}	26.4 ± 1.5
N I	953.415	1.11×10^{-2}	25.8 ± 9.9	Ar I	1066.660	6.65×10^{-2}	8.9 ± 2.9
N I	953.655	2.13×10^{-2}	25.1 ± 5.1	Fe II	1144.938	1.06×10^{-1}	11.8 ± 2.2

[a]Uncertainties are 2σ.

Table 4. Column Densities

Species	# of Detected Lines	Log(Column Density)[a] (cm^{-2})
H I	21	18.6 ± 0.4[b]
D I	4	14.05 ± 0.05
C II	1	15.9 ± 0.7
C III	1	15.4 ± 0.7
N I	10	14.62 ± 0.07
N II	2	14.90 ± 0.35
O I	16	15.51 ± 0.06
P II	1	12.08 ± 0.13
S II	2	14.02 ± 0.09[c]
Ar I	2	13.26 ± 0.12
Fe II	1	13.08 ± 0.13

[a]2σ uncertainties.

[b]Consistent with a more precise EUVE value of 18.85 ± 0.12 (Napiwotzki et al. 1996).

[c]Measured from GHRS data.

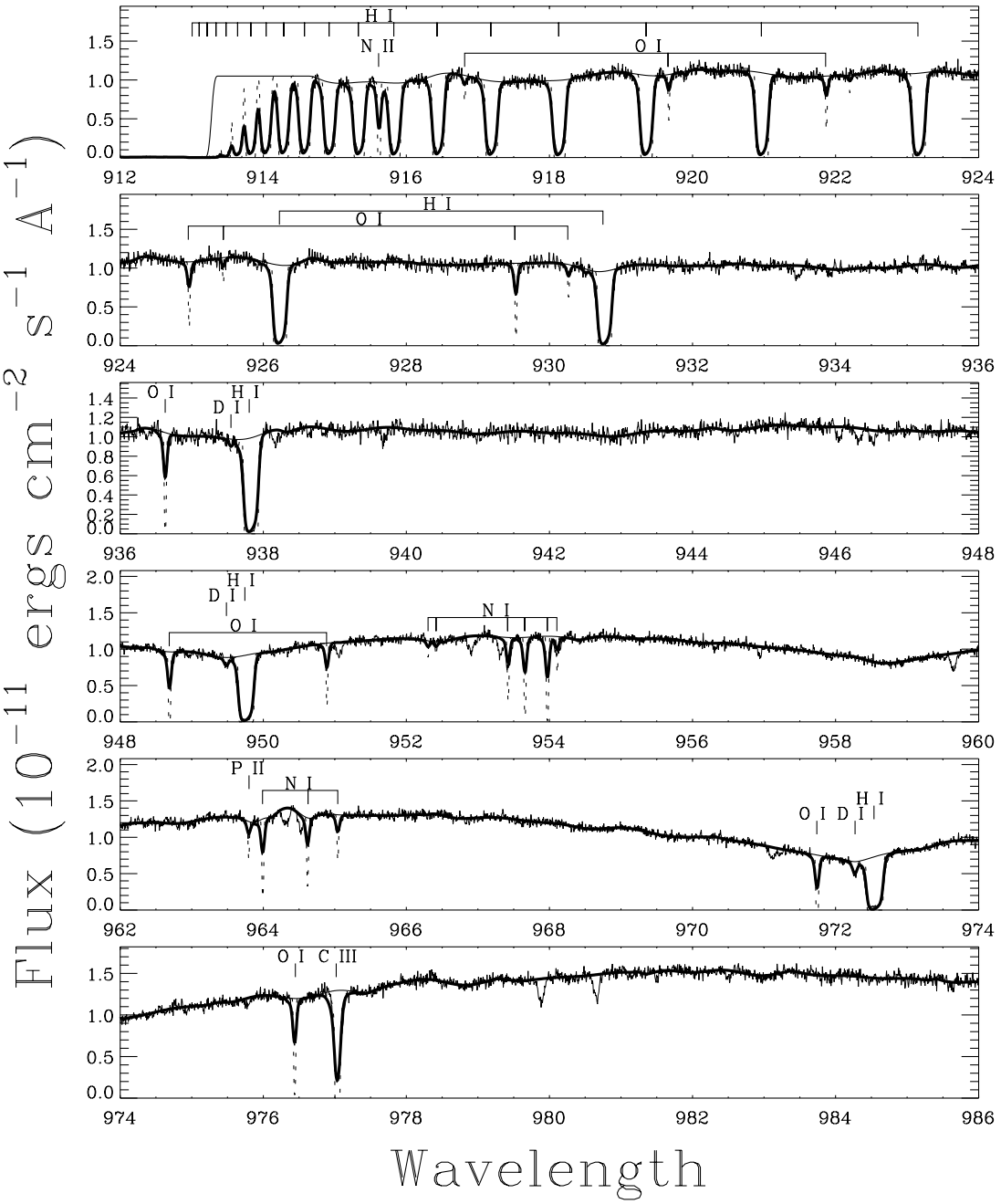

Fig. 1.— Selected regions of the LWRS WD 1634-573 spectrum observed by FUSE containing various ISM absorption features, although the Lyβ line is actually MDRS data (see text). Also shown is a global single component fit to the absorption lines, where the dotted and thick solid lines are the fit before and after convolution with the instrumental profile, respectively. The instrumental profile is a free parameter of the fit.

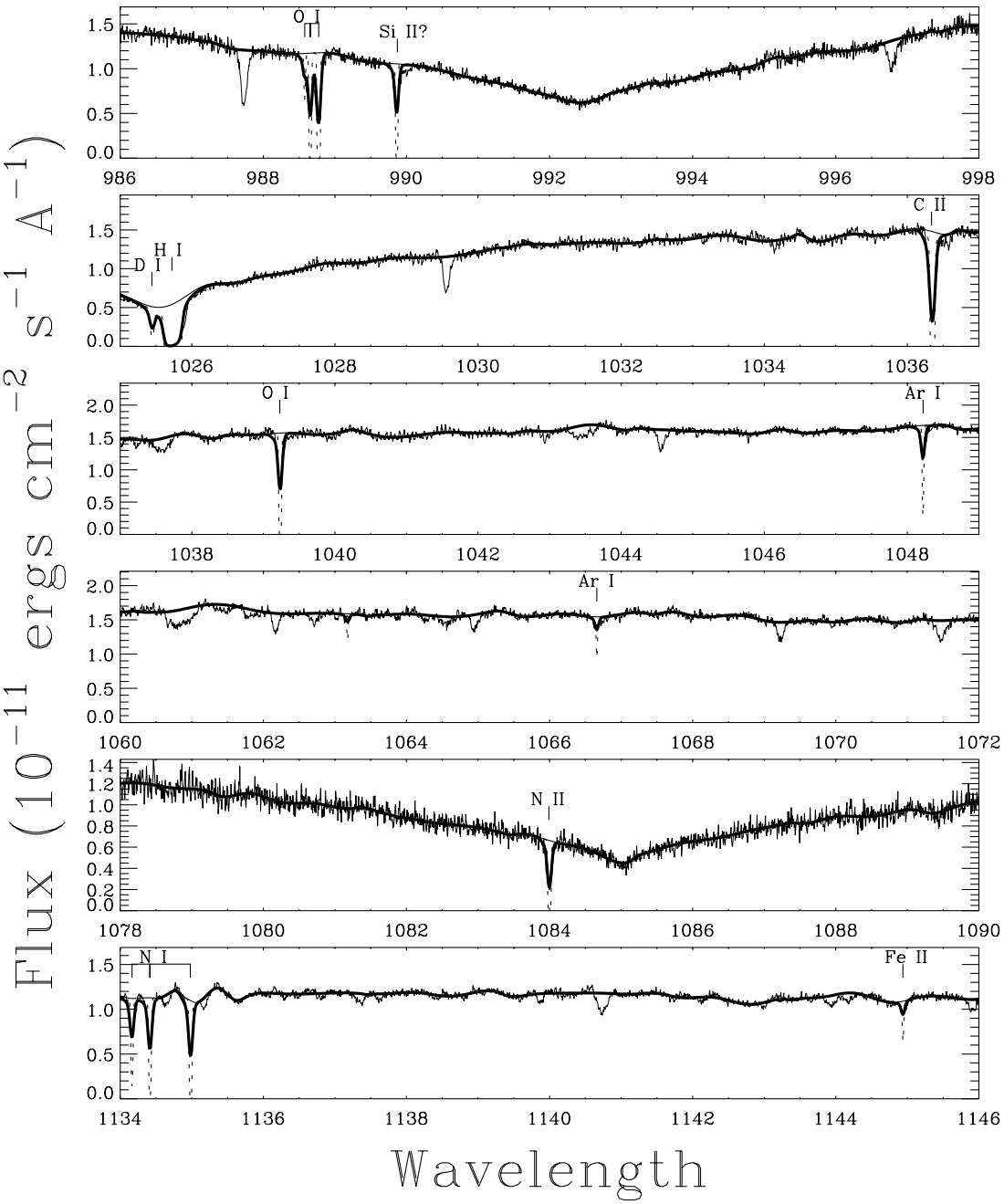

Fig. 1.— (continued)

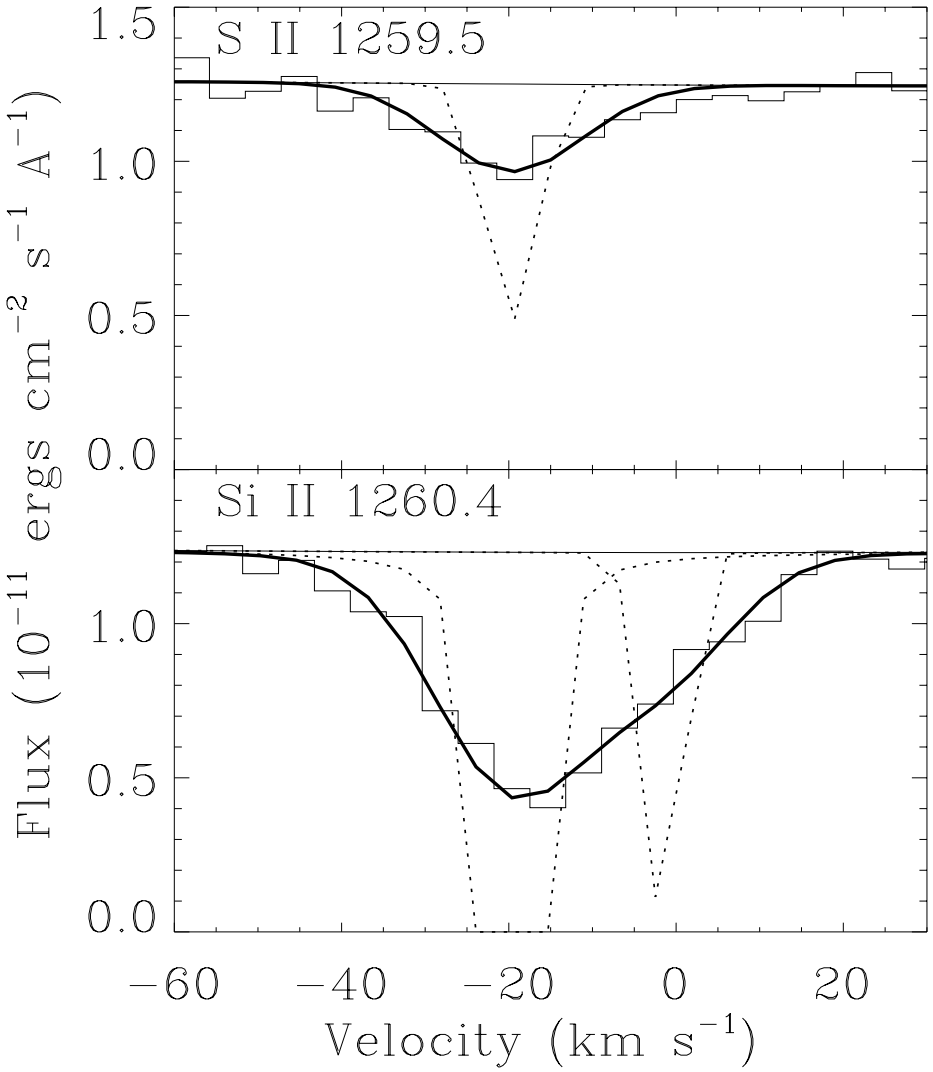

Fig. 2.— HST/GHRS moderate resolution spectra of the interstellar S II λ1259.519 and Si II λ1260.422 absorption lines observed toward WD 1634-573, plotted on a heliocentric velocity scale. The S II line is fitted with a single absorption component, where the dotted and thick solid lines are the fit before and after convolution with the instrumental profile, respectively. The opaque Si II line is fitted with two absorption components, with one forced to be at the same velocity as the single component seen for S II.

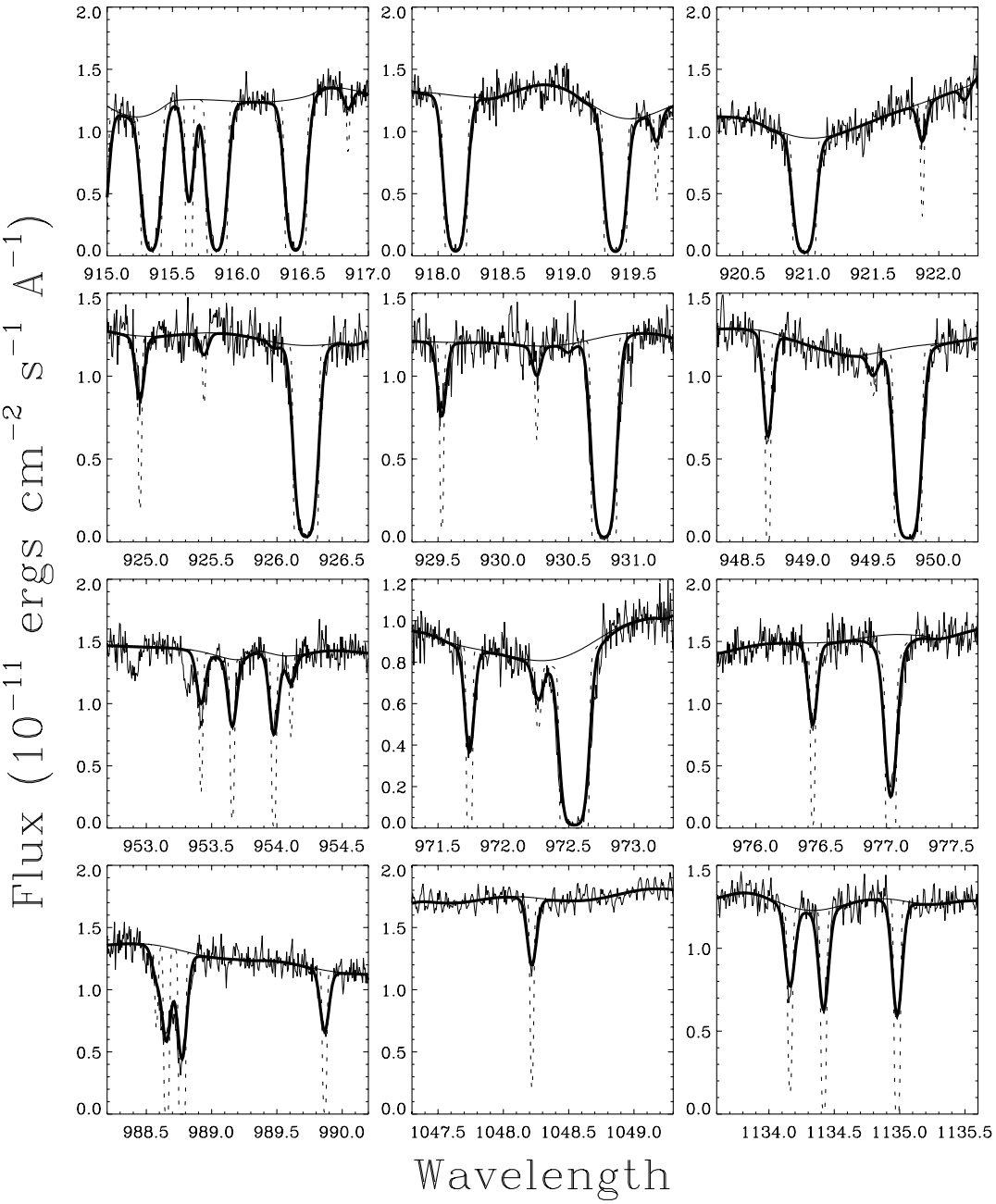

Fig. 3.— Closeups of selected lines in the MDRS WD 1634-573 spectrum observed by FUSE. See Fig. 1 or Table 2 for line identifications. Also shown is a global single component fit to the absorption lines, where the dotted and thick solid lines are the fit before and after convolution with the instrumental profile, respectively.

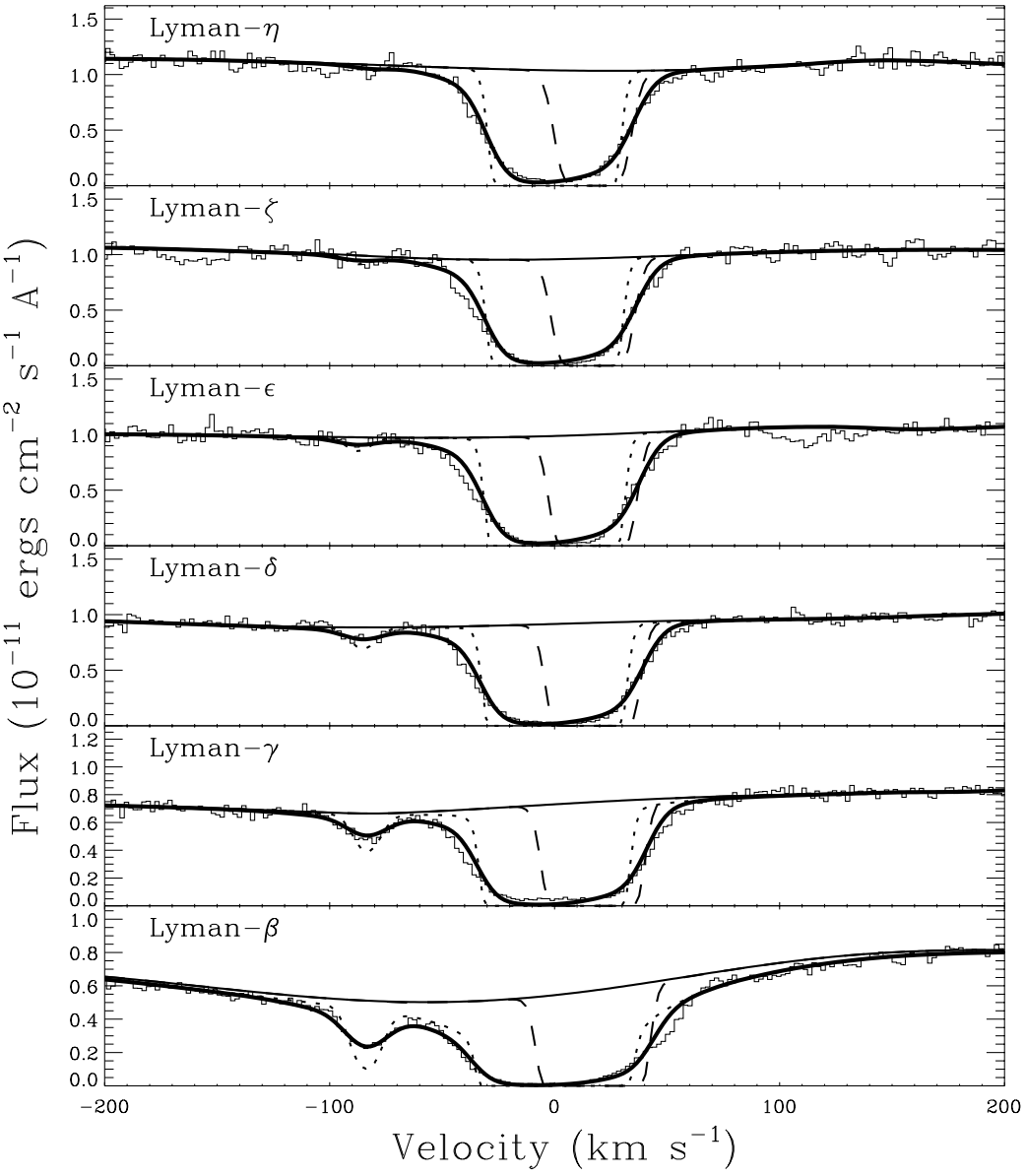

Fig. 4.— The H I and D I Lyman lines observed by FUSE using the LWRS aperture, except for Lyman-β, which is MDRS data. A two-component fit to these lines is shown, which is actually part of a global fit to all the ISM lines. The dotted and dashed lines are the individual components, while the thick solid line is the combination of the two components after convolution with the instrumental profile, which is a free parameter of the fit.

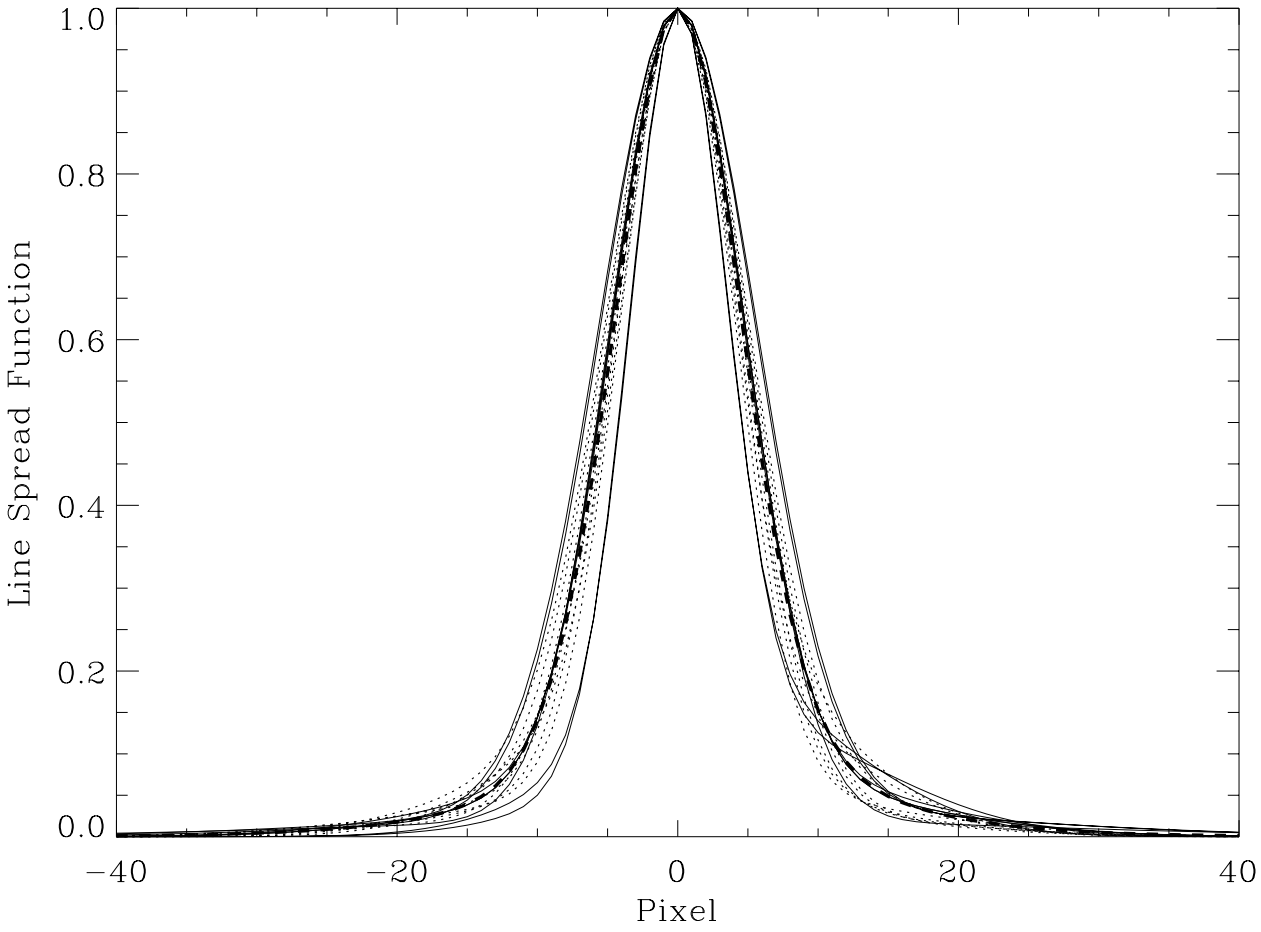

Fig. 5.— Various line spread functions derived from analyses of LWRS (solid lines) and MDRS (dotted lines) observations of WD 1634-573 and WD 2211-495. The thick dashed line is the average LSF. Two Gaussian fit parameters for this average LSF are provided in the text.